Human Motion Analysis via Statistical Motion Processing and Sequential Change Detection

Alexia Briassouli, Vagia Tsiminaki, Ioannis Kompatsiaris
Informatics and Telematics Institute
Centre for Research and Technology Hellas
Thermi-Thessaloniki, 57001, Greece
{abria,vagiula,ikom}@iti.gr

Abstract

The widespread use of digital multimedia in applications such as security, surveillance and the semantic web, has made the automated characterization of human activity necessary. In this work, a method for the characterization of multiple human activities based on statistical processing of the video data is presented. First the active pixels of the video are detected, resulting in a binary mask called the Activity Area. Sequential change detection is then applied to the data examined in order to detect at which time instants there are changes in the activity taking place. This leads to the separation of the video sequence into segments with different activities. The change times are examined for periodicity or repetitiveness in the human actions. The Activity Areas and their temporal weighted versions, the Activity History Areas, for the extracted subsequences are used for activity recognition. Experiments with a wide range of indoors and outdoors videos of various human motions, including challenging videos with dynamic backgrounds, demonstrate the proposed system's good performance.

I. Introduction

The area of human motion analysis is one of the most active research areas in computer vision, with applications in numerous fields such as surveillance, content-based retrieval, storage, virtual reality and many others. A wide range of methods has been developed over the years to deal with problems like human detection, tracking, recognition, the analysis of activity in video and the characterization of human motions [1].

One large category of approaches for the analysis of human motions is structure-based, using cues from the human body for tracking and action recognition [2]. The human body can be modeled in 2-D or 3-D, with or without explicit shape models [3]. Model-based methods include the representation of humans as stick figures [4], cardboard models [5], volumetric models [6], as well as hybrid methods that track both edges and regions [7]. Structure-based approaches that do not use explicit models detect features [8], objects [9], or silhouettes [10], which are then tracked and their motion is classified. Feature-based methods are sensitive to local noise and occlusions, and the number of features is not always sufficient for tracking or recognition. Statistical shape models such as Active Contours have also been examined for human motion analysis [11], but they are sensitive to occlusions and require good initialization.

Another large category of approaches extracts cues about the activity taking place from motion information [12]. One such approach examines the global shape of motion features, which are found to provide enough information for recognition [13]. The periodicity of human motions is used in [14] to derive templates for each action class, but at a high computational cost, as it is based on the correlation of successive video frames. In [15] actions are modeled by temporal templates, i.e. binary and grayscale masks that characterize the area of activity. Motion Energy Images (MEIs) are binary masks indicating which pixels are active throughout the video, while Motion History Images (MHIs) are grayscale, as they incorporate history information, i.e. which pixels moved most recently. This approach is computationally efficient, but cannot deal with repetitive actions, as their signatures overwrite each other in the MHI. In [16], spatiotemporal information from the video is used to create “space-time shapes” which characterize human activities in space and time. However, these spatio-temporal characteristics are specific to human actions, limiting the method to this domain only. Additionally, the translational component of motions cannot be dealt with in [16].

Both structure and motion information can be taken into account for human action analysis using Hidden Markov Models (HMMs), which model the temporal evolution of events [17], [18]. However, the HMM approach requires significant training to perform well [19] and, like all model-based methods, its performance depends on how well the chosen model parameters represent the human action.

In this work, a novel, motion-based non-parametric approach to the problem of human motion analysis is presented. Since it is not model-based, it does not suffer from sensitivity to the correct choice of model, nor is it constrained by it. Additionally, it is based on generally applicable statistical techniques, so it can be extended to a wide range of videos, in various domains. Finally, it does not require extensive training for recognition, so it is not computationally intensive, nor dependent on the training data available.

A. *Proposed framework*

The proposed system is based on statistical processing of video data in order to detect times and locations of activity changes (Fig. 1). The first stage of the system involves the extraction of the Activity Area, a binary mask of pixels which are active throughout the sequence. Only these pixels are processed in the subsequent stages, leading to a lower computational cost, and also a reduction in the possibility of errors in the motion analysis. The extraction of the Activity Area can be considered as a pre-processing step, which can be omitted for real-time processing.

The second stage of the system is one of the main novel points of this framework, as it leads to the detection of changes in activity in a non ad-hoc manner. In the current literature, temporal changes in video are only found in the context of shot detection, where the video is separated into subsequences that have been filmed in different manners. However, this separation is not always useful, as a shot may contain several activities. The proposed approach separates the video in a meaningful manner, into subsequences corresponding to different activities by applying sequential change detection methods. The input, i.e. inter-frame illumination variations, is processed sequentially as it arrives, to decide if a change has occurred at each frame. Thus, changes in activity can be detected in real time, and the video sequence can then be separated into segments that contain different actions. The times of change are further examined to see if periodicity or repetitiveness is present in the actions.

After the change detection step, the data in each subsequence between the detected change points is processed for more detailed analysis of the activity in it. Activity Areas and a temporally weighted version of them called the Activity History Areas are extracted for the resulting subsequences. The shape of the Activity Areas is used for recognition of the activities taking place: the outline of each Activity Area is described by the Fourier Shape Descriptors (see Sec. V), which are compared to each other using the Euclidean distance, for recognition. When different activities have a similar Activity Area (e.g. a person walking and running), the Activity History Areas (AHAs) are used to discriminate between them, as they contain information about the temporal evolution of these actions. This is achieved by estimating the Mahalanobis distance between appropriate features of the AHAs, like their slope and magnitude (see Sec. V for details). It is important to note that Activity History Areas would have the same limitations as MHIs [15] if they were applied on the entire video sequence: the repetitions of an activity would overwrite the previous activity history information, so the Activity History Area would not provide any new information. This issue is overcome in the proposed system, as the video is already divided into segments containing different activities, so that Activity History Areas are extracted for each repeating component of the motion separately, and no overwriting takes place.

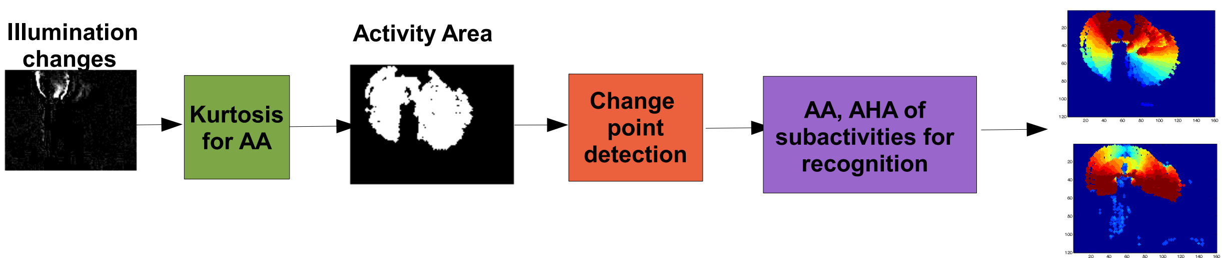

Fig. 1. Proposed system: Initially, kurtosis-based processing provides the binary Activity Area. Sequential change detection then finds change points in the video. The subsequences between the change points are processed to find their Activity Areas (AA) and Activity History Areas (AHA), that are used for activity recognition.

II. Motion Analysis: Activity Area

In the proposed system, the inter-frame illumination variations are initially processed statistically in order to find the Activity Area, a binary mask similar to the MEIs of [15], which can be used for activity recognition. Unlike the MEI, the Activity Areas are extracted via higher-order statistical processing, which makes them more robust to additive noise and small background motions. Inter-frame illumination variations, resulting from frame differences or optical flow estimates (both referred to as "illumination variations" in the sequel), can be mapped to the following two hypotheses:

$$\begin{aligned} H_0 : v_k^0(\bar{r}) &= z_k(\bar{r}) \\ H_1 : v_k^1(\bar{r}) &= u_k(\bar{r}) + z_k(\bar{r}), \end{aligned} \tag{1}$$

where $v_k^i(\bar{r}),\ i = 0, 1$ are the illumination variations for a static/active pixel respectively, at frame k and pixel $\bar{r}$. The term $z_k(\bar{r})$ corresponds to measurement noise and $u_k(\bar{r})$ is caused by pixel motion. The background is considered to be static, so only the pixels of moving objects correspond to H_1. The distribution of the measurement noise is unknown, however it can be sufficiently well modeled by a Gaussian distribution, as in [20], [21]. In the literature, the background is often modeled by mixtures of Gaussian distributions [22], but this modeling is computationally costly and not reliable in the presence of significant background changes (e.g. a change in lighting), as it does not always adapt to them quickly enough. The method used here is actually robust to deviations of the data from the simple Gaussian model [23], [24], so even in such cases, it provides accurate, reliable results at a much lower computational cost.

The illumination variations of static pixels are caused by measurement noise, so their values over time should follow a Gaussian distribution. A classical test of data Gaussianity is the kurtosis [24], which is equal to zero for Gaussian data, and defined as:

$$\mathbf{kurt}(\mathbf{y}) = \mathbf{E}[\mathbf{y^4}] - \mathbf{3}(\mathbf{E}[\mathbf{y^2}])^\mathbf{2}. \tag{2}$$

In order to find the active pixels, i.e. Activity Areas, the illumination variations at each pixel are accumulated over the entire video and their kurtosis is estimated from Eq. (2). Even if in practice the static pixels do not follow a strictly Gaussian distribution, their kurtosis is still significantly lower (by orders of magnitude) than that of active pixels. This is clearly obvious in the experimental results, where the regions of activity are indeed correctly localized, as well as in the simulations that follow.

As a practical example with a real sequence, we estimate the kurtosis of all active pixels and that of all static pixels, taken from the real video of a person boxing (Sec. VI-B), where the ground truth for the active and static pixels is extracted manually. The kurtosis of active and static pixels are plotted in Fig. 2, where it can be seen that the active pixels' kurtosis is significantly higher than that of the static pixels; note that the y-axis on Fig. 2(a) is from 0 to 4.5×10^7, while on Fig. 2(b) its range is from 0 to 10^6 (for clarity of presentation). In the static pixels of Fig. 2(b), the kurtosis is almost zero in almost all of them. It obtains higher values in pixels $8000 - 10000$, most likely due to the presence of local noise, but even these values are much lower than those of the active pixels. Indeed, the mean value of the kurtosis for the active pixels is found to be 1.34×10^6 and for the static ones it is equal to 669.54. Results like this motivate us to compare the relative values of pixels' kurtosis in practice, in order to determine if a pixel is active or static, rather than their absolute value.

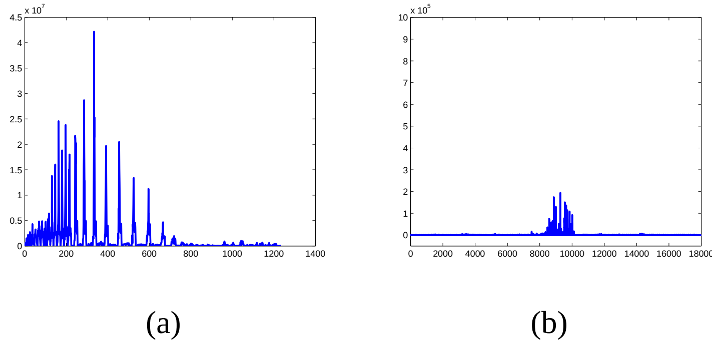

Fig. 2. Kurtosis estimates from a real video of a person boxing for (a) active and (b) static pixels.

A very common model for the background is the Mixture of Gaussians (MoG) [25], so we compare the kurtosis of data following a Gaussian, a MoG and an Exponential distribution. The exponential data is chosen as it is clearly non-Gaussian and will provide a measure of comparison for the other data. Monte Carlo simulations take place with 500 sample sets of data from each distribution, of length 5000 each. The kurtosis estimated for each sample set and for each distribution is shown in Fig. 3 where it can be seen that the Gaussian and MoG data have significantly lower kurtosis values than the Exponential (non-Gaussian) data. Indeed, the average kurtosis for the Gaussian data is -0.004, for the MoG it is -0.0084 and for the Exponential it is 5.077. Consequently, the kurtosis can reliably discriminate between active and static pixels even for background data that is modeled by a MoG instead of by a simple Gaussian.

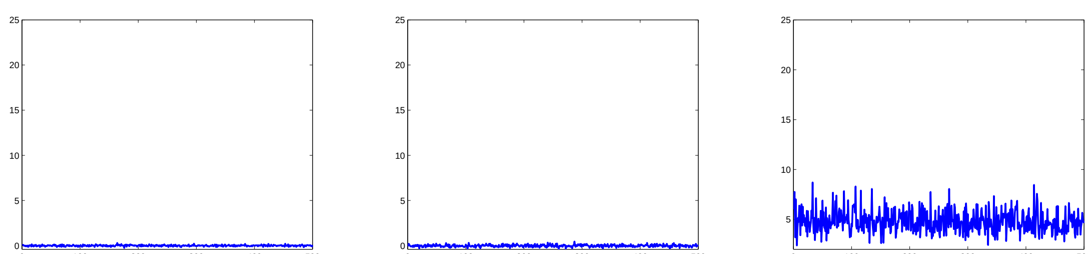

Fig. 3. Kurtosis estimates for data following a Gaussian, a MoG and an Exponential distribution.

III. Motion Analysis: Activity History Area

As mentioned in Sec. I-A, the Activity Area is not always sufficient for recognizing activities, as some actions can lead to Activity Areas with very similar shapes. For example, different translational motions like jogging, running and walking have similar Activity Areas, although they evolve differently in time. Thus, information about their temporal evolution should be used to discriminate amongst them. The temporal evolution of activities is captured by the Activity History Area (AHA), which is similar to the Motion History Area of [15], but extracted using the kurtosis, as in Sec. II, rather than straightforward frame differencing. If the Activity Area value AA (binarized kurtosis value) on pixel $\bar{r}$ is $AA(\bar{r})$ at frame t, the AHA is defined as:

$$\text{AHA}(\bar{r}, t) = \begin{cases} \tau, & \text{if AA(r)=1;} \\ \max(0, \text{AHA}(r, t-1) - 1), & \text{else.} \end{cases} \tag{3}$$

Essentially, the AHA is a time-weighted version of the Activity Area, with higher weights given to the pixels which were active more recently. This introduces information about an activity's evolution with time, which can be particularly helpful for the classification of different actions. As an example, Fig. 4 shows the Activity Area and AHA of a person running to the right and the same person running to the left. It is obvious that the direction of motion is captured by the AHA, which obtains higher values in the most recently activated pixels, but not by the Activity Area, which is a binary mask, and therefore can only provide spatial localization. In Fig. 4, the AHA values have warmer colors (darker in grayscale) for the most recently activated pixels, while cooler colors (lighter in grayscale) represent pixels that were active in the past.

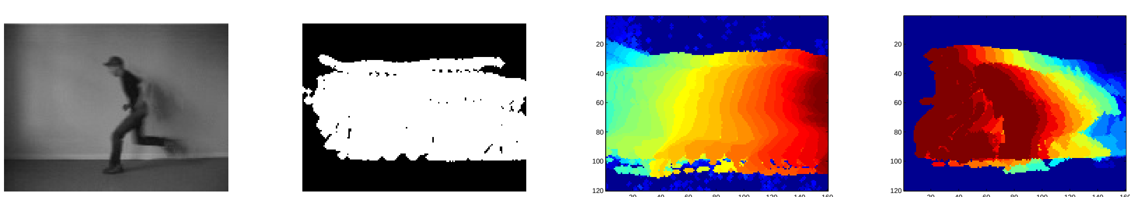

(a) (b) (c) (d)

Fig. 4. Person running. (a) Frame 10. (b) AA. AHA for motion: (c) to the right, (d) to the left. The AHA has higher values in the regions of the Activity Area that were active most recently, represented by warm colors, and lower values in pixels that were active in the past, corresponding to cooler colors.

IV. Sequential Change Detection

One of the main novel points of the proposed system is the detection of the times at which the activity taking place changes. The input data for the change detection is a sequence of illumination variations from frame k_0 to k, i.e. $\mathbf{v}_{k_0,k} = [\overline{v}_{k_0}, \overline{v}_{k_0+1}, ..., \overline{v}_k]$. If only the pixels inside the Activity Area are being examined, the data from each frame k^* contains the illumination variations of that frame's pixels, for the pixels inside the Activity Area. Thus, if the activity area contains N_a pixels, we have $\overline{v}_{k^*} = [v_{k^*}(1), ..., v_{k^*}(N_a)]$. In this work we examine the case where only the pixels inside the Activity Area are processed. It is considered that the data follows a distribution f_0 before a change occurs, and f_1 after the change, at an unknown time instant k_{ch}. This is expressed by the following two hypotheses:

$$\begin{aligned} H_0 : \mathbf{v}_{k_0,k} &\sim f_0 \\ H_1 : \mathbf{v}_{k_0,k} &\sim f_1. \end{aligned} \tag{4}$$

At each frame k, $\mathbf{v}_{k_0,k}$ is input into a test statistic to determine whether or not a change has occurred until then, as detailed in Sec. IV-A. If a change is detected, only the data after frame k is processed to detect new changes, and this is repeated until the entire video has been examined.

A. Cumulative Sum (CUSUM) for Change Detection

The sequential change detection algorithm [26] uses the log-likelihood ratio (LLRT) of the input data as a test statistic. For the detection of a change between frames k_0 and k, we estimate:

$$T_k = LLRT_k(f_1||f_0) = \ln \frac{f_1(\mathbf{v}_{k_0,k})}{f_0(\mathbf{v}_{k_0,k})} = \ln \prod_{i=k_0}^{k} \frac{f_1(\overline{v}_i)}{f_0(\overline{v}_i)} = \sum_{i=k_0}^{k} \ln \frac{f_1(\overline{v}_i)}{f_0(\overline{v}_i)}, \tag{5}$$

where it has been assumed that the frame samples $\overline{v}_i$ are identically independently distributed (i.i.d.) under each hypothesis, so that $f_H(\mathbf{v}_{k_0,k}) = \prod_{i=k_0}^{k} f_H(\overline{v}_i),\ H = 0, 1$. Similarly, it is assumed that the illumination variations of the pixels inside the Activity Area are i.i.d., so $f_H(\overline{v}_i) = \prod_{n=1}^{Na} f_H(v_i(n)),\ H = 0, 1,\ i = k_0, ..., k$.

Pixels in highly textured areas can be considered to have i.i.d. values of illumination variations, as they correspond to areas of the moving object with a different appearance, which may be subject to local sources of noise, shadow, or occlusion. In homogeneous image regions that move in the same manner this assumption does not necessarily hold, however even these pixels can be subject to local sources of noise, which remove correlations between them. The approximation of the data distribution for data that is not considered i.i.d. is very cumbersome, making this assumption necessary for practical purposes as well. Such assumptions are often made in the change detection literature to ensure tractability of the likelihood test.

Under the i.i.d. assumption, the test statistic of Eq. (5) obtains the recursive form [26]:

$$T_k = \max\left(0, T_{k-1} + \ln \frac{f_1(\overline{v}_k)}{f_0(\overline{v}_k)}\right), \tag{6}$$

where $\overline{v}_k = [v_k(1), ..., v_k(N_a)]$ is the data from the active pixels in the current frame k. Then, Eq. (5) can also be written as:

$$T_k = \sum_{i=k_0}^{k} \sum_{j=1}^{N_a} \ln \frac{f_1(v_i(j))}{f_0(v_i(j))}, \tag{7}$$

and Eq. (6) becomes:

$$T_k = \max\left(0, T_{k-1} + \sum_{j=1}^{N_a} \ln \frac{f_1(v_k(j))}{f_0(v_k(j))}\right). \tag{8}$$

A change is detected at this frame when the test statistic becomes higher than a pre-defined threshold. Unlike the threshold for sequential probability likelihood ratio testing [27], [28], the threshold for the CUSUM testing procedure cannot be determined in a closed form manner. It has been proven in [29] that the optimal threshold for the CUSUM test for a pre-defined false alarm γ is the threshold that leads to an average number of changes equal to γ under H_0, i.e. when there are no real changes. In the general case examined here, the optimal threshold needs to be estimated empirically from the data being analyzed [30]. In Sec VI we provide more details about how we determine the threshold experimentally.

In practice, illumination variations of only one pixel over time do not provide enough samples to detect changes effectively, so the illumination variations of all active pixels in each frame are used. If an Activity Area contains N_a pixels, this gives $N_a \times (k - k_0 + 1)$ samples from frame k_0 to k, which leads to improved approximations of the data distributions, as well as better change detection performance.

B. Data Modeling

As Eq. (6) shows, in order to implement the CUSUM test, knowledge about the family of distributions before and after the change is needed, even if the time of change itself is not known.

For the case where only the pixels in the Activity Area are being examined, it is known that they are active, and hence do not follow a Gaussian distribution (see Sec. II). The distribution of active pixels over time contains outliers introduced by a pixel's change in motion, which lead to a more heavy-tailed distribution than the Gaussian, such as the Laplacian or generalized Gaussian [31]. The Laplacian distribution is given by:

$$f(x) = \frac{1}{2b}\exp\left(-\frac{|x-\mu|}{b}\right), \tag{9}$$

where μ is the data mean and $b = \sigma/\sqrt{2}$ is its scale, for variance σ^2. The tails of this distribution decay more slowly than those of the Gaussian, since its exponent contains an absolute difference instead of the difference squared. Its tails are consequently heavier, indicating that data following the Laplace distribution contains more outlier values than Gaussian data. The test statistic of Eq. (7) for N data samples can then be written as:

$$\begin{aligned} T_k &= \sum_{i=k_0}^{k}\sum_{j=1}^{N_a}\ln\left[\frac{b_0}{b_1}\exp\left(-\frac{|v_i(j)-\mu_1|}{b_1}+\frac{|v_i(j)-\mu_0|}{b_0}\right)\right] \\ &= NN_a\ln\frac{b_0}{b_1}+\sum_{i=k_0}^{k}\sum_{j=1}^{N_a}\left(-\frac{|v_i(j)-\mu_1|}{b_1}+\frac{|v_i(j)-\mu_0|}{b_0}\right) \end{aligned} \tag{10}$$

In order to verify the validity of the Laplacian approximation of the data, the illumination variations are modeled by the Gaussian and Laplacian distributions, and their accuracy is compared. The generalized Gaussian model is not examined, as its approximation is computationally costly and hence impractical. Fig. 5 contains plots showing the distribution of the actual data in comparison with its approximation by a Gaussian and Laplacian distribution. The Root Mean Square error (RMS) between the actual empirical data distribution and the corresponding Gaussian and Laplacian model is presented in Table I for several videos, where it can be seen that the Laplacian distribution provides a better fit. Modeling experiments are conducted on all the videos used in the experiments, but have not been included in Table I for reasons of space and readability. The mean RMS estimated from all the video sequences examined is 0.0915 for the Gaussian and 0.0270 for the Laplacian model, justifying the choice of the latter as a better fit for our data. The data could be modeled even more accurately by heavier tailed distributions, such as alpha-stable distributions [32]. However, these do not exist in closed form, so they cannot be used in the likelihood ratio test. A closed form distribution from the alpha-stable family, namely the Cauchy, describes the data well in the DCT domain [33], but the Laplacian has been shown to better describe quantized image data [34].

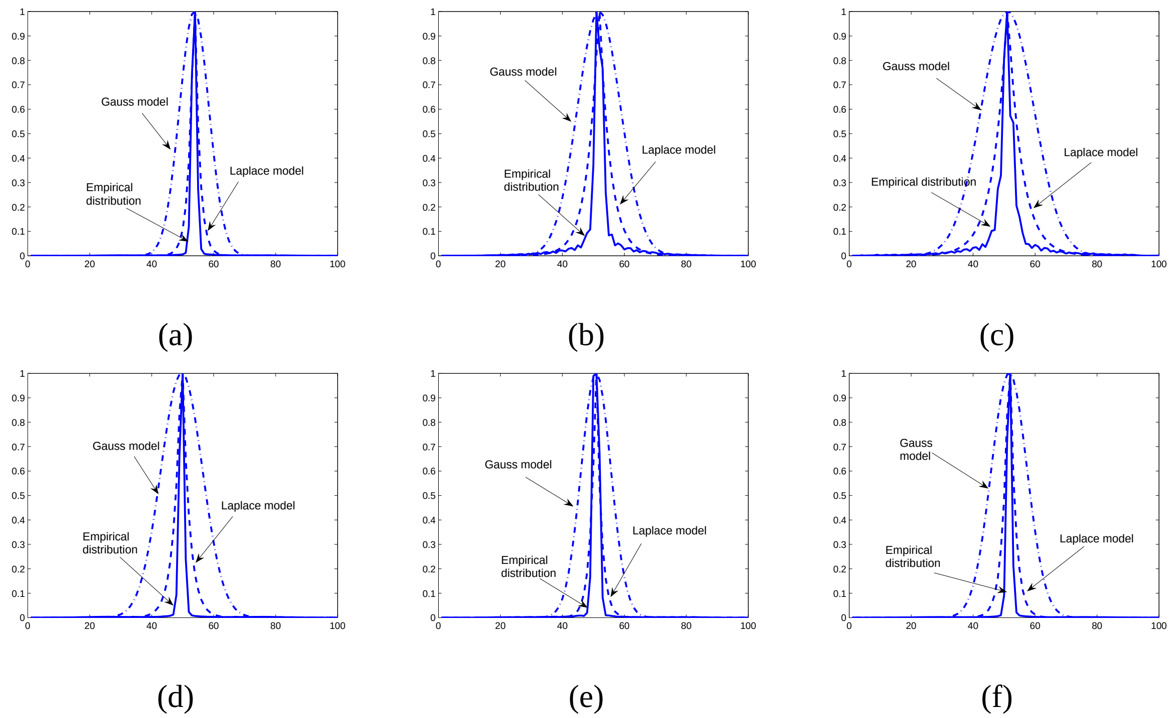

Fig. 5. Empirical distribution, Laplace and Gaussian data modeling for: (a) Daria Jump, (b) Denis Jack, (c) Eli Jump in place, (d) Moshe Run (e) Daria Walk (f) Moshe Skip.

V. Recognition

The proposed system detects when activities change in a video, based on sequential processing of the inter-frame illumination variations. After change points are detected, the subsequences resulting inbetween them are further processed in order to characterize and recognize the activities taking place in them. We focus on the case where there is a pre-processing stage that extracts the active pixels, as this reduces the system's overall computational cost and increases its reliability, since it does not look for activity changes in static pixels. The complete system consists of the following stages:

1) Activity areas are extracted to find the active pixels.
2) The illumination variations of the pixels inside the activity area over time are estimated.
3) Sequential change detection is applied to the illumination variations, to detect changes.

TABLE I

GAUSSIAN AND LAPLACE MODELING ERRORS

Model/Video	Lyova Run	Eli Run	Daria Run	Denis Run	Moshe Run	Shahar Run	Lena2 Run
Gaussian	0.0913	0.0976	0.1077	0.0898	0.1010	0.0975	0.1128
Laplace	0.0239	0.0265	0.0344	0.0253	0.0310	0.0295	0.0409
Model/Video	Lena1 Run	Ira Run	Ido Run	Daria Jack	Denis Jack	Eli Jack	Ido Jack
Gaussian	0.1206	0.0801	0.0933	0.1026	0.1031	0.1105	0.0879
Laplace	0.0433	0.018	0.0253	0.0371	0.0333	0.042	0.0257
Model/Video	Ira Jack	Lena Jack	Lyova Jack	Moshe Jack	Shahar Jack	Daria Jump	Denis Jump
Gaussian	0.1129	0.0864	0.108	0.1081	0.1057	0.0815	0.0734
Laplace	0.047	0.0307	0.0359	0.0368	0.0383	0.0179	0.0153
Model/Video	Eli Jump	Ido Jump	Ira Jump	Lena Jump	Lyova Jump	Moshe Jump	Shahar Jump
Gaussian	0.094	0.0827	0.0680	0.0956	0.0788	0.0947	0.0984
Laplace	0.0228	0.0237	0.0219	0.0239	0.0207	0.027	0.0234

4) If the change points are (nearly) equidistant, the motion is considered to be (near) periodic.
5) The Activity Areas and Activity History Areas for the frames (subsequences) between change points are extracted. The shape of the Activity Areas and the direction and magnitude of motion are derived from the Activity History Area, to be used for recognition.
6) False alarms are removed: if motion characteristics of successive subsequences are similar, those subsequences are merged and the change point between them is deleted.
7) Multiple Activity Areas and Activity History Areas originating from the same activity are detected and merged if their motion and periodicity characteristics coincide.
8) Shape descriptors of the resulting Activity Areas and motion information from the Activity History Areas are used for recognition.

The detection of different activities between change points increases the usefulness and accuracy of the system for many reasons. The proposed system avoids the drawback of “overwriting” that characterizes MHIs that are extracted using the entire sequence. In periodic motions, for example, where an activity takes place from left to right, then from right to left and so on, all intermediate changes of direction are lost in the temporal history image if the all video frames are used. This is overcome in our approach, as Activity History Areas are estimated over segments with one kind of activity, giving a clear indication of the activity's direction and temporal evolution. This also allows the extraction of details about the activity taking place, such as the direction of translational motions, periodicity of motions like boxing, or of more complex periodic motions, containing similarly repeating components (see Sec. VI-B). Finally, the application of recognition techniques to the extracted sequences would not be meaningful if the sequence had not been correctly separated into subsequences with one activity each.

Both the shape of the Activity Area and motion information from the Activity History Area are used for accurate activity recognition, as detailed in the sections that follow.

A. *Fourier Shape Descriptors of Activity Area*

The shape of the Activity Areas can be described by estimating the Fourier Descriptors (FD) [35] of their outlines. The FDs are preferred as they provide better classification results than other shape descriptors [36]. Additionally, they are rotation, translation and scale invariant, and inherently capture some perceptual shape characteristics: their lower frequencies correspond to the average shape, while higher frequencies describe shape details [36]. The FDs are derived from the Fourier Transform (FT) $F_1, F_2, ..., F_N$ of each shape outline's boundary coordinates. The DC component F_1 is not used, as it only indicates the shape position. All values are divided by the magnitude of $|F_1|$ to achieve scale invariance, and rotation invariance is guaranteed by using their magnitude. Thus, the FDs are given by:

$$\bar{f} = \left[\frac{|F_2|}{|F_1|}, \frac{|F_3|}{|F_1|}, ..., \frac{|F_N|}{|F_1|}\right]. \tag{11}$$

Only the 20 first terms of the FD, corresponding to the 20 lowest frequencies, are used in the recognition experiments, as they capture the most important shape information. The comparison of the FDs for different activities takes place by estimating their Euclidean distance, since they are scale, translation and rotation invariant. When $L = 20$ elements of the FDs are retained, the Euclidean distance between two FDs $\bar{f}_A$, $\bar{f}_B$ is given by:

$$d_{Eucl} = \sum_{k=1}^{L} |\bar{f}_A(k) - \bar{f}_B(k)|. \tag{12}$$

and each activity is matched to that with the shortest Euclidean distance.

B. Activity History Area for motion magnitude and direction detection

Although the shape of Activity Areas is characteristic of many activities and is effectively used for their recognition, there also exist categories of activities with very similar Activity Areas. A characteristic example commonly encountered in practice is that of translational motions, whose Activity Area covers a linear region (horizontally, vertically, or diagonally). It is seen in Fig. 6, 14(e)-(g) that this shape is linear for different translational motions, such as walking or running, so it is insufficient for discriminating amongst them. However, this linearity property can be used to separate translations from other kinds of motions. The linearity can be derived from its mean in the horizontal direction. Activities that do not contain a translational component, such as waving lead to a local concentration of pixel activity, which makes sense since they take place over a confined area (last image pairs of Fig. 6).

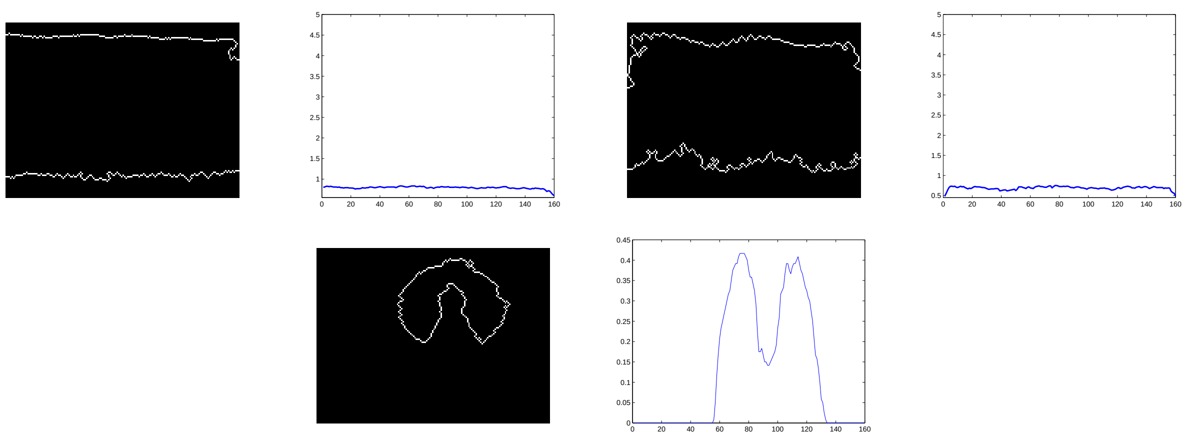

Fig. 6. Activity Area outlines and their mean in horizontal direction for walking, running, waving. The mean AA outline is linear for translational motions.

In order to separate translational motions from each other, the Activity History Areas (Fig. 7) are used. Motion direction and magnitude information is extracted by estimating the mean of the Activity History Area in the horizontal and vertical directions. In this work all translational motions are horizontal, so only the horizontal mean of the AHA is estimated. This mean forms a line whose slope provides valuable information about the direction and magnitude of motion:

- The sign of the slope shows the direction of motion: it is negative for a person moving to the left and positive for motion to the right.

- The magnitude of the slope is inversely proportional to the velocity, i.e. higher magnitudes correspond to slower activities.

The values of the Activity History Area are higher in pixels that were active recently; here the the pixel locations correspond to the horizontal axis, and the slope is estimated by:

$$slope = \frac{t_{last} - t_{first}}{x_{last} - x_{first}}, \tag{13}$$

where t_{first} is the frame at which the first horizontal pixel (the leftmost x location here) is activated, and t_{last} the frame where the last horizontal pixel is activated (the rightmost x location). This can be seen in Figs. 8(a), (b) for motions to the right and left respectively: motion to the right leads to a positive slope since the rightmost pixel is activated at the most recent frame, while motion to the left leads to a negative slope.

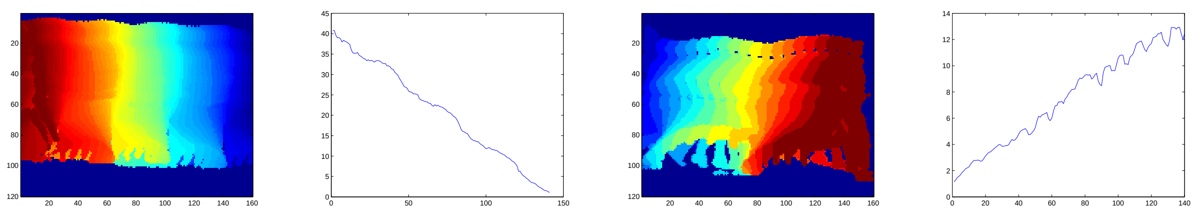

Fig. 7. Activity History Areas and their means for translational motions to the left and right: walking left, running right. Direction and magnitude information is included in these areas.

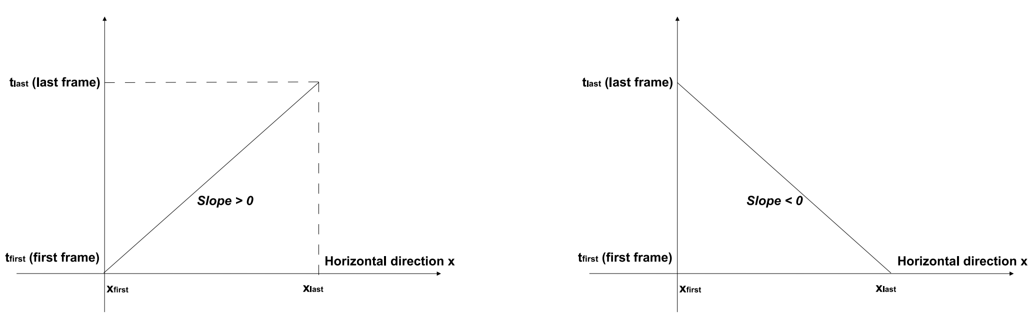

Fig. 8. Mean of Activity History Area in horizontal direction for motion to the right and left.

The Activity History Area of a fast activity (e.g. running) contains a small range of frames (from t_{first} to t_{last}), since it takes place in a short time, whereas the Activity History Area of a

TABLE II

SLOPE MAGNITUDE OF MEAN AHA FOR BASELINE TRANSLATIONAL VIDEOS

Motion	Run	Jog	Walk
AHA slope	0.1192 ± 0.0358	0.1651 ± 0.0455	0.27248 ± 0.054625

slow activity occurs during more frames, since the motion lasts longer. In order to objectively discriminate between fast and slow actions, the same number of pixels must be traversed in each direction. Thus, in Eq. (13), $x_{last} - x_{first}$ is the same for all activities, and $t_{last} - t_{first}$ has high values for slow actions and low values for fast ones. Consequently, higher magnitudes of the slope of Eq. (13) correspond to slower motions and lower magnitudes correspond to faster ones.

The activities examined are horizontal walking, jogging, running, and cover the same distance, so that the slope magnitude can be objectively used to discriminate amongst them. For comparison, the Activity History Area is extracted from a set of baseline translation videos, and its horizontal mean is estimated. The slope of the mean is found from Eq. (13) and its magnitude is given in Table II for each activity. As expected, the slope has higher values for slower motions.

For the classification of a test video, its Activity History Area is extracted, and its mean is estimated. The sign of its slope indicates whether the person is moving to the right or left and its magnitude is compared to the average slope of the three baseline categories of Table II using the Mahalanobis distance. For a baseline set with mean $\mu = [\mu_1, ..., \mu_N]$ and covariance matrix Σ, the Mahalanobis distance of data $y = [y_1, ..., y_N]$ from it is defined as $d_{Mahal}(y) = \sqrt{(y-\mu)^T \Sigma^{-1} (y-\mu)}$. The Mahalanobis distance is used as a distance metric as it incorporates data covariance, which is not taken into account by the Euclidean distance. In this case the data is one dimensional (the slope) so its variance is used instead of the covariance matrix.

VI. EXPERIMENTS FOR RECOGNITION

Experiments with real videos take place to examine the performance of the change detection module. These videos can be found on http://mklab.iti.gr/content/temporal-templates-human-activity-recognition, so that the reader can observe the ground truth and verify the validity of the experiments. The ground truth for the times of change is extracted manually and compared to the estimated change points to evaluate the detection performance.

We model the data by a Laplacian distribution (Sec. IV-B) to approximate f_0 and f_1 of Eq. (5), which are unknown and need to be estimated from the data $\mathbf{v}_{k_0,k}$ at each time k. The distribution of the "current" data f_0 is extracted from the first w_0 samples of $\mathbf{v}_{k_0,k}$, in order to take into account samples that belong to the old distribution, while f_1 is approximated using the most recent w_1 samples. There could be a change during the first w_0 samples used to approximate f_0, but there is no way to determine this a priori, so there is the implicit assumption that no change takes place in the first w_0 frames. Currently, there is no theoretically founded way to determine the optimal length of the windows w_0 and w_1, as stated in the change detection literature [37]. Consequently, the best possible solution is to empirically determine the window lengths that give the best change detection results for certain categories of videos, and use them accordingly. After extensive experimentation, $w_0 = 10$ and $w_1 = 5$ are found to give the best detection results with the fewest false alarms, for detecting a change between successive activities. For periodic motions, the changes occur more often, so smaller windows are used, namely $w_0 = w_1 = 4$.

At each frame k, the test statistic T_k is estimated and compared against a threshold in order to determine whether or not a change has occurred. Due to the sequential nature of the system, there is no closed form expression for this threshold, so an optimal value cannot be determined for it a priori [38]. It is found empirically that for videos of human motions like the ones examined here, the threshold which leads to the highest detection rate with the fewest false alarms is given by:

$$\eta_{opt} = \mu_T + 2.3 \cdot \sigma_T, \tag{14}$$

where μ_T and σ_T are the mean and standard deviation of the test statistic T_k until frame k.

A. Experiments with translational motions

In this section, experimental results for videos containing translational motions, namely walking, jogging and running, are presented. Characteristic frames of some videos, the corresponding activity area and the likelihood ratio over time are shown in Fig. 9 and all the videos examined can be seen on http://mklab.iti.gr/content/temporal-templates-human-activity-recognition. The activity areas correctly capture the pixels that are active in each video and the likelihood ratio values change at the time when the actual change occurs. In total, change points are correctly detected for 16 videos with translational motions, as shown in Table III, but for three of the videos false alarms are also detected. These false alarms are easily eliminated by examining the average motion and its variance for each extracted subsequences as they do not change significantly before and after a false alarm. In this manner, no false alarms remain and only the correct change points are detected, shown in bold fonts in Table III (for the cases where there were false alarms). In the table, LR indicates that an activity takes place from left to right, HD means “horizontally-diagonally”, LRL is left-right-left and LRLR is left-right-left-right. The numbers (e.g. Jog LR1) distinguish between different videos of the same activity. The last two videos, Walk LRL and Walk LRLR have two and three change points respectively, which are correctly detected in both cases, with no false alarms.

Fig. 9(e)-(i) contains frames from a walking sequence, where the pixels around the person’s neck are mistaken for static pixels, leading to two Activity Areas, one corresponding to the head and one to the body, shown in Fig. 9(f), (g). When there are more than one Activity Areas, the sequential testing is applied to each Activity Area separately, since there could be more than one different activity taking place. In this example the area corresponding to the head is too small to provide enough samples for a reliable estimate of the change-point, so only the likelihood ratio values for the Activity Area corresponding to the body of the person with the coat are shown in Fig. 9(h), (i). Even in this case, the change points are correctly found.

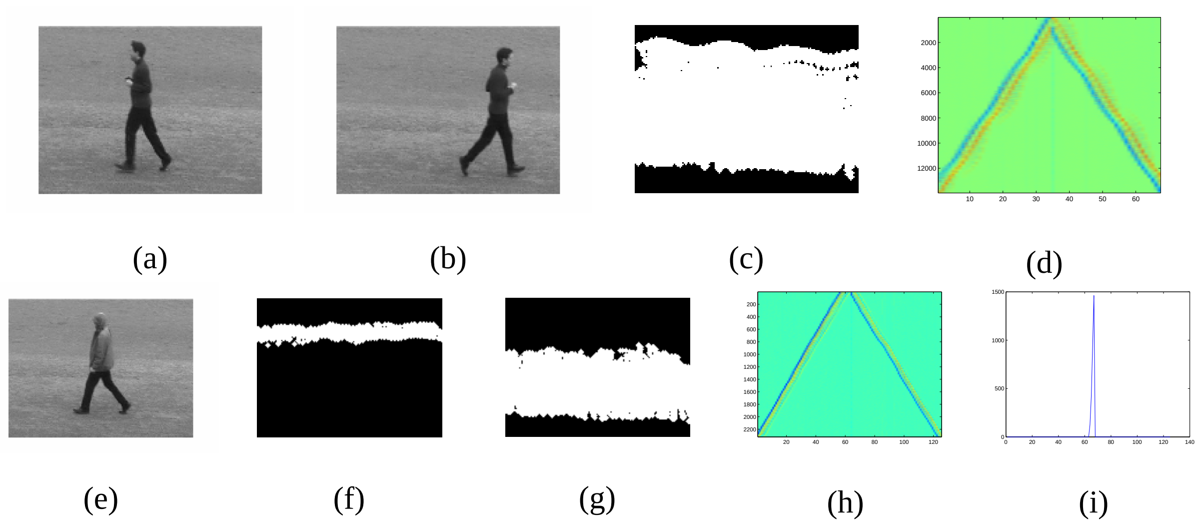

Fig. 9. (a), (b) Frames of person jogging left, right. (c) Activity area. (d) Likelihood ratio values for each active pixel, over all frames. (e) Person walking left, right. (f), (g) Activity areas for head and body. (h) Likelihood ratio (LRT) values for each active pixel (in the body area), over all frames. (i) LRT values for all pixels (in the body area), showing change times.

TABLE III

CHANGE POINTS FOR VIDEOS WITH TRANSLATIONAL MOTIONS

Video	Jog LR 1	Jog LR 2	Run LR 1	Run LR 2	Walk HD	Walk LR 1	Walk LR 2	Walk LR 3
Change points	35	33	23	20	57	58	61	18, 30, **89**
Video	Walk LR 4	Walk LR 5	Walk LR 6	Walk LR 7	Walk LR 8	Walk LR 9	Walk LRL	Walk LRLR
Change points	37-**93**-134	**58**-71	49	67	74	70	58, 102	35, 69, 104

B. Experiments with non-translational motions

Combinations of non-translational motions are examined in this section. The first video contains a person clapping, followed by a person boxing, and the second shows a person waving followed by a person clapping (see Fig. 10 and http://mklab.iti.gr/content/temporal-templates-human-activity-recognition). The resulting Activity Areas contain the pixels that move in both activities and the likelihood ratio values estimated over all active pixels lead to correct change point detection. For the clapping-boxing sequence the correct change point is detected at frame 99, but there are also false alarms at frames $65, 85, 123, 159, 176, 200$, introduced because of changes in the individual repeating activities (clapping only or boxing only). As in Sec VI-A, these false alarms are eliminated by simply estimating the motion characteristics of the extracted subsequences, which undergo significant change only at frame 99. In the handwaving-handclapping video, the true change point is found at frame 127, but false alarms are also detected at frames $11, 35, 56, 75, 89, 141, 225$, which are removed as before, leading to the detection of only the correct change point. It should be emphasized that the relative height of the likelihood ratio values is not taken into account for the elimination of false alarms. Instead, the motion characteristics of the resulting subsequences are measured, as explained above.

Periodic Motions:

The values of the data windows w_0, w_1, chosen for approximating f_0, f_1 respectively, affect the resolution of the system. When w_0, w_1 have higher values, they detect changes at a coarse granularity, but at the cost of missing small changes inside each individual activity. In this section we present experiments where these windows are set to $w_0 = w_1 = 4$, enabling the detection of changes in repeating activities with good accuracy.

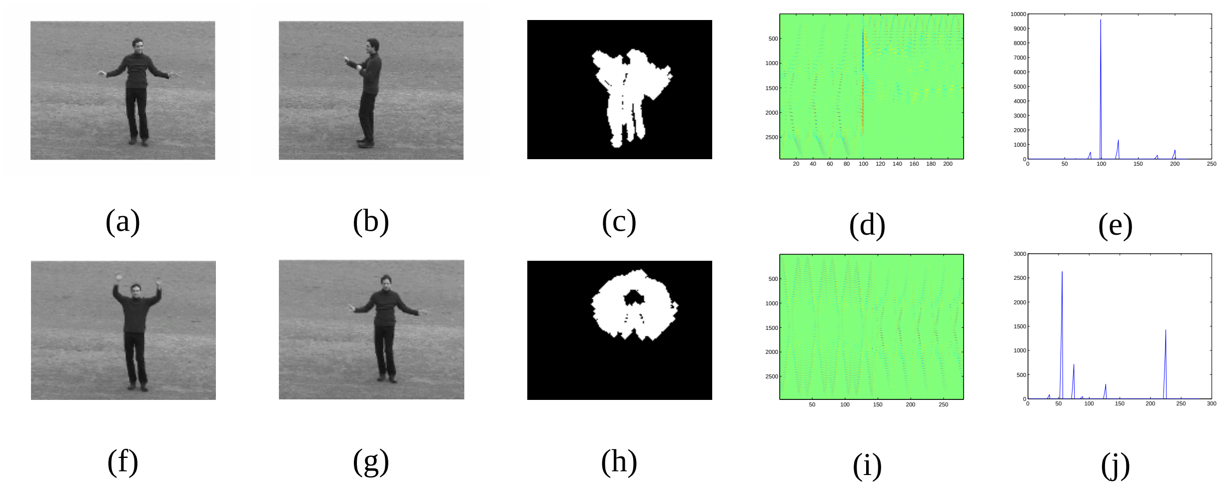

Fig. 10. Handclapping-boxing video: (a) frame 30, (b) frame 100. (c) Activity area of clapping and boxing. (d) Likelihood ratio estimated for each pixel. (e) Likelihood ratio values for all pixels. Handwaving-handclapping video: (f) frame 10, (g) frame 254. (h) Activity area. (i) Likelihood ratio estimated for each pixel. (j) Likelihood ratio values for all pixels, used for change detection.

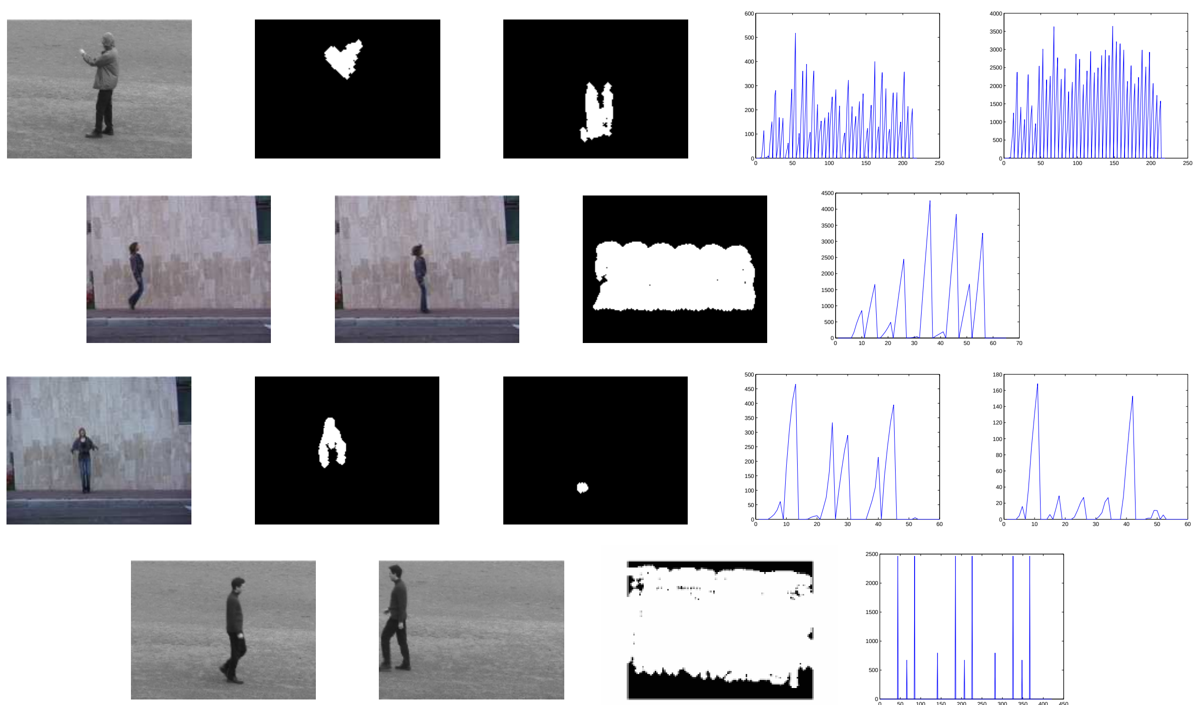

Fig. 11. First row: Boxing. Second row: Jumping. Third row: Jumping in place. Fourth row: Composite walking sequence. Each row shows video frames, the activity area, likelihood ratio values for all pixels.

TABLE IV

CHANGE POINTS FOR PERIODIC MOTIONS, EXTRACTED PERIOD

Video	Change points	Period
Box	8, 13, 18, 23,..., 203, 208, 213	5
Jump	10, 15, 20, 15,...,46, 51, 56	5
Jump in place	6, 11, 18, 26, 34, 42, 50	8
Walk	22, 19, 56, 44, 22, 19, 56, 44, 22, 19, 56, 44	3

Fig. 11 shows frames of the videos examined, along with the corresponding activity areas, and log-likelihood ratio values. For the Boxing and Jumping in Place videos, two activity areas are extracted, one corresponding to the upper part of the human's body and one to the legs. This is because the middle area of the body is relatively static. For those cases each activity area is examined separately: the resulting change points for the two activity areas coincide, and the motion characteristics between these change points are the same, so these areas are (correctly) assigned to the same activity. Table IV shows the detected change points for each video and the resulting period. The last video is more complex, containing 3 identical subsequences of a person walking left-right-left: all change points are found, and form a pattern that repeats 3 times.

C. Experiments with multiple Activity Areas

A video of two people performing different activities at different, but overlapping, time intervals, is examined (Fig. 12, top two rows). The Activity Area consists of two distinct binary masks, corresponding to the different activities, so the sequential change detection takes place in each area separately. For both Activity Areas, the likelihood ratios for all pixels inside them correctly locate the times of change at frames $53, 81, 97$ for the person walking on the left, and at frame 33 for the person walking on the right. Two more complicated videos, with multiple but overlapping activity areas are examined (Fig. 12, last two rows). In this case there is only one activity area, containing more than one activities, but the proposed method can still detect the changes of each activity. This is because enough of the data being processed undergoes a change, which is then detected by the sequential likelihood test. In the first video, with the crossing ladies, changes are found at frames $35, 81$ when one lady enters and when another leaves, respectively. In the second video with the beach scene, changes are detected at frame 37, when the two ladies disappear behind the umbrella, at frame 52 when the three ladies meet, frame 66 when one lady is hidden by the umbrella, 78 when the girl reappears, and 94 when the two walking ladies disappear (see http://mklab.iti.gr/content/temporal-templates-human-activity-recognition). This shows that the proposed system can handle cases of multiple activities taking place during different, possibly overlapping, intervals, with accurate results. Also, these videos contain dynamically moving backgrounds, and yet accurate change detection is obtained for them.

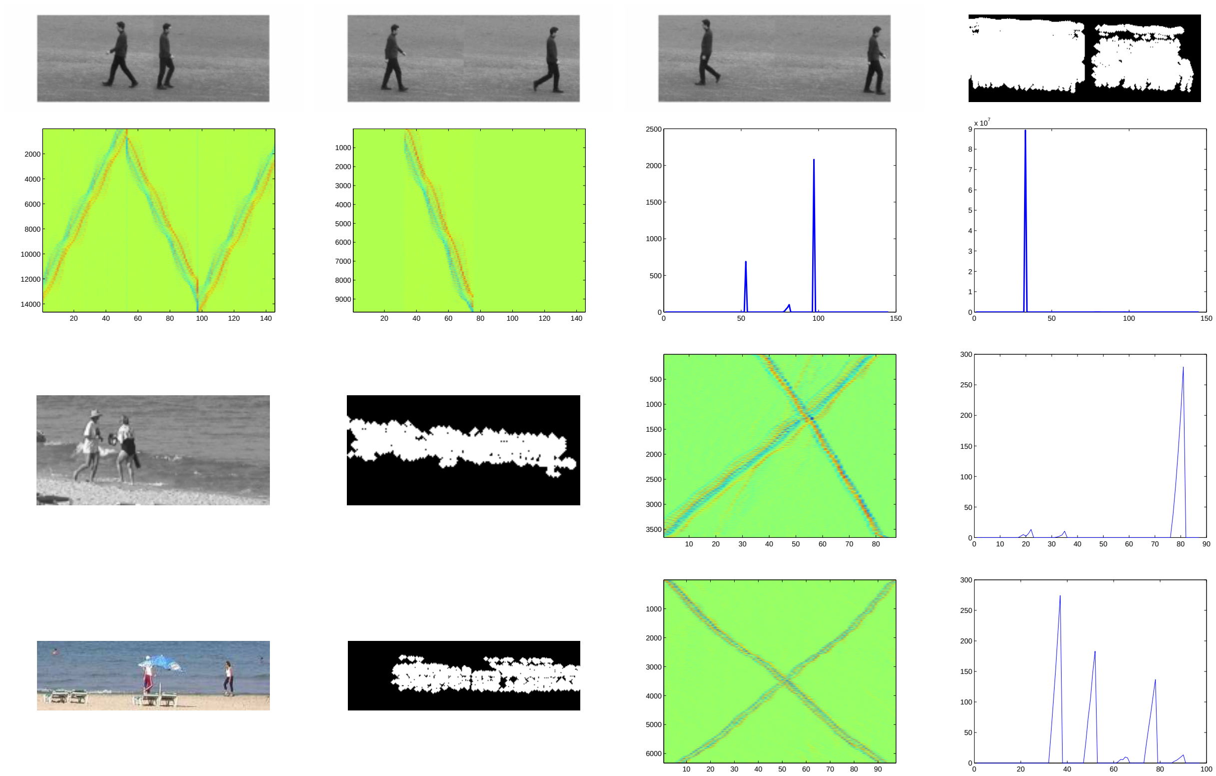

Fig. 12. Videos with multiple Activity Areas. First two rows, people walking, two separate activity areas. Third row, crossing ladies. Fourth row, beach. The activity area from rows 3 and 4 contains both motions, but change points are correctly found. Each row shows video frames, the activity area, likelihood ratio values and likelihood ratio values for all pixels.

D. Experiments with Dynamic Backgrounds

Several challenging videos involving dynamic backgrounds are examined. Despite the moving background, the activity areas are found with accuracy, as seen in Fig. 13. The change detection results are extracted from the last column of Fig. 13 and are tabulated in Table V. All change points are detected correctly, along with a few false alarms, which are in italics in Table V. The false alarms are easily removed by comparing the motion characteristics between estimated change points: before and after a false alarm, the motion characteristics do not change, so those change points are eliminated.

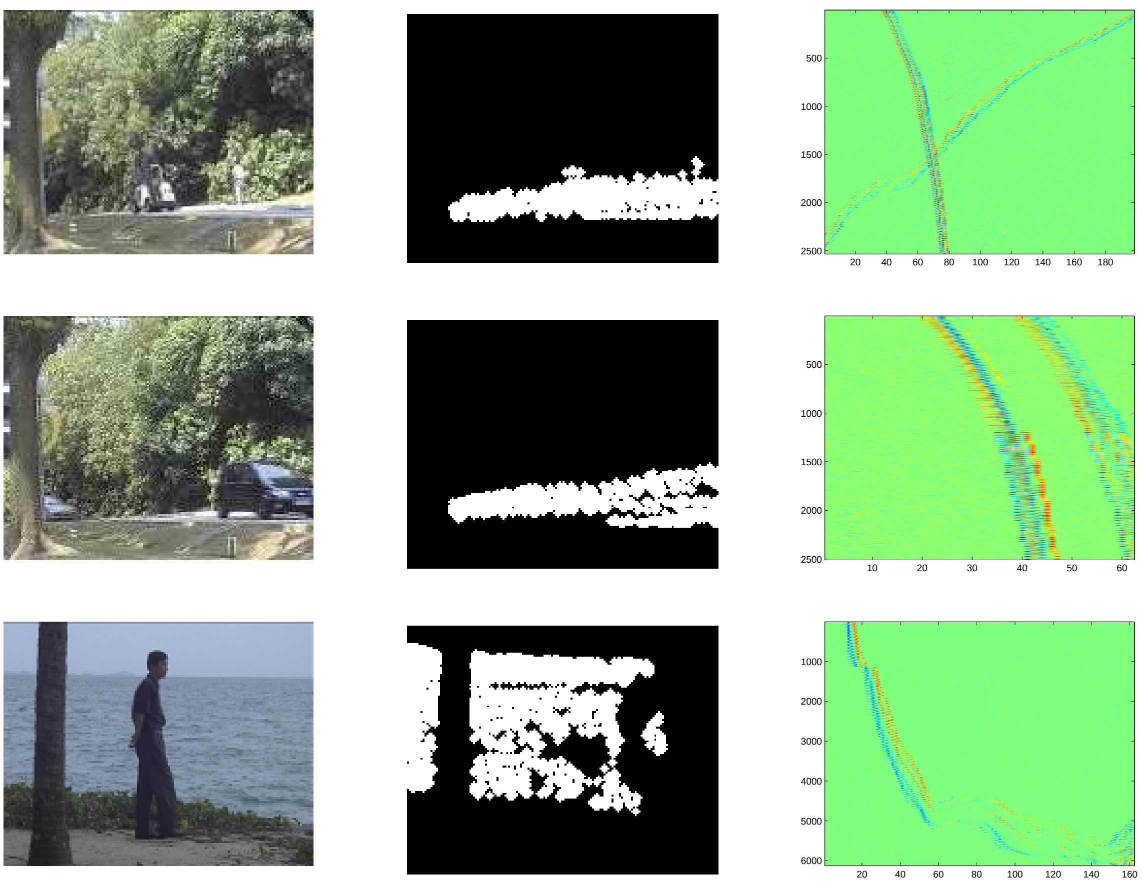

Fig. 13. Videos with dynamic backgrounds. First two rows, videos with trees moving in the wind, last row a video with moving water surface. Each row shows video frames, activity area, likelihood ratio values, likelihood ratio values for all pixels.

TABLE V

CHANGE POINTS FOR DYNAMIC BACKGROUNDS

Video	Change points
Trees 2	*23*, 39, 61, 72, 80
Trees 5	15, 62, 77, 87, *110*, 130, 153
Trees 6	*14*, 28
Trees 7	*10*, *17*, 23, 37, 45, *56*
Water surface	13, *40*, 58, 68, 81, *110*, 121, *133*, 146

VII. EXPERIMENTS FOR RECOGNITION

Experimental results for recognition based on the Activity Area and Activity History Area information are presented here. It should be emphasized that the activity recognition results are good although there is no training stage, so the proposed method is applicable to various kinds of activity, without restrictions imposed by the training set.

A. *Recognition using Fourier Shape Descriptors of Activity Area*

Experiments for activity recognition take place for boxing, handclapping and handwaving, with Activity Area outlines like those in Fig. 14(a)-(f). The comparison of the FDs for 23 videos of boxing, handclapping and handwaving each, lead to the correct classification of 75.49% of the boxing, 79.45% of the handclapping and 87.15% of the handwaving sequences as can be seen in Table VI. This makes intuitive sense, as the outlines of the Activity Areas for the boxing videos have a blob-like shape, which is not as descriptive as the other boundaries. Indeed, the best recognition results are achieved for the handclapping video, whose Activity Area outlines have a very characteristic shape. Additionally, the boxing and handclapping motions are more often confused with each other than with the handwaving, as expected, since the latter's Activity Area has a very distinctive shape.

Different methods have also used this dataset for activity recognition. In [39], excellent recognition results of 98% for boxing, 91.9% for clapping and 91.7% for waving are achieved. However, that method is based on extracting motion templates (motion images and motion context) using very simple processing, which would fail for more challenging sequences, like

TABLE VI

RECOGNITION FOR BOXING, HANDCLAPPING, HANDWAVING (%)

Activity	Box	Handclap	Handwave
Box	**75.49**	24.51	0
Handclap	17.39	**79.45**	3.16
Handwave	0	12.85	**87.15**

those in Sec. VI-D: the standard deviation of the illumination over successive video frames is estimated to find active pixels, a measure which can easily lead to false alarms in the presence of noise. In [40], Support Vector Machines (SVMs) are used, so training is required in their method. They achieve recognition of 97.9% for boxing, but 59.7% for clapping and 73.6% for waving, i.e. worse than our results. Finally, in [41] volumetric features are used, leading to a higher computational cost, but achieving recognition results of only 69.4% for boxing, 55.6% for clapping and 91.7% for waving (which is comparable to our result). Overall our approach has a consistently good performance, with recognition rates above 75%, despite its simplicity, low computational cost, and the fact that it does not require any training or prior knowledge.

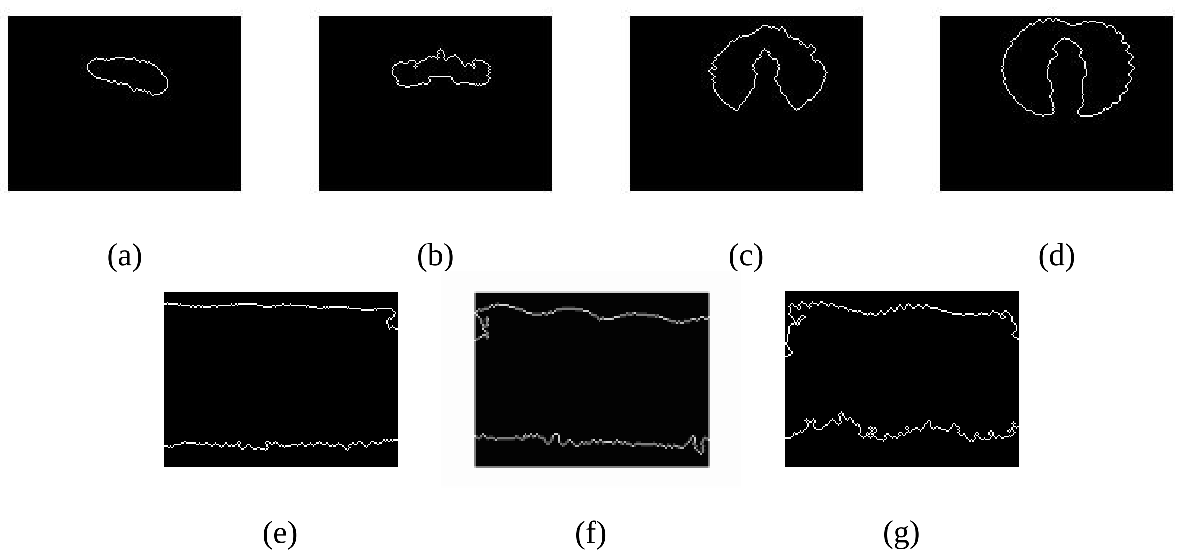

Fig. 14. Activity Area outlines for (a) boxing, (b) clapping, (c), (d) waving, (e) walking, (f) jogging, (g) running.

TABLE VII

MAHALANOBIS DISTANCE FOR RUNNING VIDEOS

Motion	Run 1 left	Run 1 right	Run 2 left	Run 2 right
AHA slope	-0.1030	0.0801	-0.0794	0.0822
d_{Mahal} from Run	0.4524	1.0926	1.1122	1.0339
d_{Mahal} from Jog	1.3661	1.8695	1.8849	1.8233
d_{Mahal} from Walk	3.1026	3.5218	3.5346	3.4834

TABLE VIII

MAHALANOBIS DISTANCE FOR JOGGING VIDEOS

Motion	Jog 1 left	Jog 1 right	Jog 2 left	Jog 2 right
AHA slope	-0.1602	0.1527	-0.1438	0.1448
d_{Mahal} from Run	1.1467	0.9370	0.6882	0.7162
d_{Mahal} from Jog	0.1088	0.2736	0.4693	0.4473
d_{Mahal} from Walk	2.0554	2.1927	2.3557	2.3374

B. Recognition using Activity History Area Features

For translational motion classification, we examine the subsequences extracted from the walking, jogging and running videos of Sec VI-A after change detection. The direction of motion in each one is correctly found for all data. The Mahalanobis distance of the slope magnitude from the test values for each video is shown in Tables VII- IX, where it can be seen that correct classification is achieved in all cases, both for the direction and for the type of motion.

VIII. CONCLUSIONS

In this work, a novel approach for the analysis of human motion in video is presented. The kurtosis of inter-frame illumination variations leads to binary masks, the Activity Areas, that indicate which pixels are active throughout the video. The temporal evolution of the activities is characterized by temporally weighted versions of the Activity Areas, the Activity History Areas. Changes in the activity taking place are detected via sequential change detection, applied on the inter-frame illumination variations. This separates the video into sequences containing different

TABLE IX

MAHALANOBIS DISTANCE FOR WALKING VIDEOS

Motion	Walk 1 L	Walk 1 R	Walk 2 L	Walk 2 R	Walk 3 L	Walk 3 R	Walk 4 L	Walk 4 R
AHA slope	-0.3138	0.4112	-0.3676	0.3511	-0.3518	0.3887	-0.2729	0.3980
d_{Mahal} from Run	5.4408	8.1638	6.9449	6.4836	6.5032	7.5348	4.2974	7.7948
d_{Mahal} from Jog	3.2675	5.4085	4.4501	4.0874	4.1028	4.9139	2.368	55.1183
d_{Mahal} from Walk	0.7565	2.5395	1.7414	1.4393	1.4521	2.1276	0.0077	2.2979

activities, based on changes in their motion. The activity taking place in each subsequence is then characterized by the shape of its Activity Area or on its magnitude and direction, derived from the Activity History Area. For non-translational activities, Fourier Shape Descriptors represent the shape of each Activity Area, and are compared with each other, for recognition. Translational motions are characterized based on their relative magnitude and direction, which are retrieved from their Activity History Areas. The combined use of the aforementioned recognition techniques with the proposed sequential change detection for the separation of the video in sequences containing separate activities leads to successful recognition results at a low computational cost. Future work includes the development of more sophisticated and complex recognition methods, so as to achieve even better recognition rates. The application of change detection on video is also to be extended to a wider range of videos, as it is a generally applicable method, not limited to the domain of human actions.

ACKNOWLEDGMENTS:

The research leading to these results has received funding from the European Communitys Seventh Framework Programme FP7/2007-2013 under grant agreement FP7-214306 - JUMAS, from FP6 under contract number 027685-MESH and FP6-027026-K-Space.

REFERENCES

[1] L. Wang, W. Hu, , and T. Tan, “Recent developments in human motion analysis,” *Pattern Recogn.*, vol. 36, pp. 585618, 2003.

[2] J. K. Aggarwal and Q. Cai, “Human motion analysis: a review,” *Comput. Vis. Image Understand.*, vol. 73, no. 3, pp. 428–440, 1999.

[3] D. M. Gavrila, “The visual analysis of human movement: A survey,” *Comput. Vis. Image Understand.*, vol. 72, no. 1, pp. 8298, 1999.

[4] K. Akita, “Image sequence analysis of real world human motion,” *Pattern Recogn.*, vol. 17, no. 1, pp. 73–83, Aug. 1984.

[5] I. Haritaoglu, D. Harwood, and L. S. Davis, “W4: Real-time surveillance of people and their activities,” *IEEE Transactions on Pattern Analysis and Machine Intelligence*, vol. 22, no. 8, pp. 809–830, Aug. 2000.

[6] A. Bottino and A. Laurentini, “A silhouette based technique for the reconstruction of human movement,” *Comput. Vis. Image Understand.*, vol. 83, pp. 7995, 2001.

[7] R. D. Green and L. Guan, “Quantifying and recognizing human movement patterns from monocular video imagespart I: A new framework for modeling human motion,” *IEEE Transactions on Circuits and Systems for Video Technology*, vol. 14, no. 2, pp. 179189, Feb. 2004.

[8] I. Laptev and T. Lindeberg, “Space-time interest points,” in *Proc. of Int. Conf. on Computer Vision*, 2003, pp. 432–439.

[9] M. Oren, C. Papageorgiou, P. Sinha, E. Osuna, and T. Poggio, “Pedestrian detection using wavelet templates,” in *Proc. of Int. Conf. on Computer Vision*, 1997, pp. 193–199.

[10] M. Singh, A. Basu, and M. Mandal, “Human activity recognition based on silhouette directionality,” *IEEE Transactions on Circuits and Systems for Video Technology*, vol. 18, no. 9, pp. 1280–1292, Sep. 2008.

[11] T. Cootes, C. Taylor, D. Cooper, and J. Graham, “Active shape models - their training and applications,” *Comput. Vis. Image Understand.*, vol. 61, no. 1, pp. 38–59, 1995.

[12] C. Cedras and M. Shah, “Motion-based recognition: a survey,” *Image Vis. Comput.*, vol. 13, no. 2, pp. 129–155, 1995.

[13] J. Boyd and J. Little, “Global versus structured interpretation of motion: moving light displays,” in *Proc. of Int. Conf. on Pattern Recognition*, 1997, pp. 18–25.

[14] R. Polana and R. Nelson, “Detecting activities,” in *Proc. of Int. Conf. on Pattern Recognition*, 1993, pp. 2–7.

[15] A. F. Bobick and J. W. Davis, “The recognition of human movement using temporal templates,” *IEEE Transactions on Pattern Analysis and Machine Intelligence*, vol. 23, no. 3, pp. 257–267, Mar. 2001.

[16] L. Gorelick, M. Blank, E. Shechtman, M. Irani, and R. Basri, “Actions as space-time shapes,” *IEEE Transactions on Pattern Analysis and Machine Intelligence*, vol. 29, no. 12, pp. 2247–2253, December 2007.

[17] J. Yamato, J. Obya, and K. Ishii, “Recognizing human action in time sequential images using hidden markov model,” in *Proc. of Int. Conf. on Computer Vision*, 1992, pp. 379–385.

[18] A. Kale, A. Sundaresan, A. N. Rajagopalan, N. P. Cuntoor, A. K. RoyChowdhury, V. Kruger, and R. Chellappa, “Identification of humans using gait,” *IEEE Transactions on Image Processing*, vol. 13, no. 9, pp. 1163–1173, Sep. 2004.

[19] X. Sun, C. W. Chen, and B. S. Manjunath, “Probabilistic motion parameter models for human activity recognition,” in *Proc. of Int. Conf. on Pattern Recognition*, Aug. 2002, vol. 1, p. 443446.

[20] C.R. Wren, A. Azarbayejani, T.J. Darrell, and A.P. Pentland, “Pfinder: real-time tracking of the human body,” *IEEE Transactions on Pattern Analysis and Machine Intelligence*, vol. 19, no. 7, pp. 780–785, 1997.

[21] T. Aach, L. Dumbgen, R. Mester, and D. Toth, “Bayesian illumination-invariant motion detection,” in *Proceedings IEEE International Conference on Image Processing (ICIP)*, October 2001, vol. 3, pp. 640–643.

[22] C. Stauffer and W. Grimson, “Adaptive background mixture models for real-time tracking,” in *Computer Vision and Pattern Recognition, 1999. Proceedings CVPR ’99, 1999 IEEE Computer Society Conference on*, June 1999.

[23] M.E. Hassouni, H. Cherifi, and D. Aboutajdine, “Hos-based image sequence noise removal,” *IEEE Transactions on Image Processing*, vol. 15, no. 3, pp. 572–581, 2006.

[24] G.B. Giannakis and M. K. Tsatsanis, “Time-domain tests for Gaussianity and time-reversibility,” *IEEE Transactions on Signal Processing*, vol. 42, no. 12, pp. 3460–3472, Dec. 1994.

[25] C. Stauffer and W.E.L. Grimson, “Adaptive background mixture models for real-time tracking,” in *Proc. IEEE Conf. Computer Vision Patt. Recog.*, June 1999, pp. 246–252.

[26] E. S. Page, “Continuous inspection scheme,” *Biometrika*, vol. 41, no. 1, pp. 100–115, June 1954.

[27] H. V. Poor, *An Introduction to Signal Detection and Estimation*, Springer-Verlag, New York, 2nd edition, 1994.

[28] A. Wald, *Sequential Analysis*, Dover Publications, 2004.

[29] G. V. Moustakides, “Optimal stopping times for detecting changes in distributions,” *Ann. Statist.*, vol. 14, no. 4, pp. 1379–1387, 1986.

[30] M. Basseville and I. Nikiforov, *Detection of Abrupt Changes: Theory and Application*, Prentice-Hall, Inc., Englewood Cliffs, N.J., 1993.

[31] B. Aiazzi, L. Alparone, and S. Baronti, “Estimation based on entropy matching for generalized gaussian pdf modeling,” *IEEE Transactions on Signal Processing*, vol. 6, no. 6, pp. 138–140, 1999.

[32] J. P. Nolan, *Stable Distributions - Models for Heavy Tailed Data*, Birkhäuser, Boston, 2010, In progress, Chapter 1 online at academic2.american.edu/$\sim$jpnolan.

[33] A. Briassouli, P. Tsakalides, and Athanasios Stouraitis, “Hidden messages in heavy-tails:DCT-domain watermark detection using alpha-stable models,” *IEEE Transactions on Multimedia*, vol. 7, pp. 700 715, Aug. 2005.

[34] D. Simitopoulos, S. A. Tsaftaris, N. V. Boulgouris, A. Briassouli, and M. G. Strintzis, “Fast watermarking of MPEG-1/2 streams using compressed-domain perceptual embedding and a generalized correlator detector,” *EURASIP JASP*, vol. 8, pp. 1088–1106, 2004.

[35] M. Bober, “MPEG-7 visual shape descriptors,” *IEEE Transactions on Circuits and Systems for Video Technology*, vol. 11, no. 6, pp. 716–719, 2001.

[36] D. S. Zhang and G. Lu, “A comparative study of Fourier descriptors for shape representation and retrieval,” in *Proc. of the Fifth Asian Conference on Computer Vision (ACCV02)*, Jan. 2002, pp. 646–651.

[37] C. Hory, A. Kokaram, and W.J. Christmas, “Threshold learning from samples drawn from the null hypothesis for the generalized likelihood ratio CUSUM test,” in *Machine Learning for Signal Processing, 2005 IEEE Workshop on*, Sept. 2005, pp. 111–116.

[38] I.V. Nikiforov, “A generalized change detection problem,” *IEEE Transactions on Information Theory*, vol. 41, no. 1, pp. 171 – 187, Jan. 1995.

[39] Z.M. Zhang, Y.Q. Hu, S. Chan, and L.T. Chia, “Motion context: A new representation for human action recognition,” in *European Conference on Computer Vision 2008*, 2008, pp. 817–829.

[40] C. Schuldt, I. Laptev, and B. Caputo, “Recognizing human actions: A local SVM approach,” in *Proceedings ICPR 2004*, 2004.

[41] Y. Ke, R. Sukthankar, and M. Hebert, “Efficient visual event detection using volumetric features,” in *International Conference on Computer Vision*, October 2005, vol. 1, pp. 166 – 173.